Journal of Sound and Vibration (2001) **244**(1), 35–56
doi:10.1006/jsvi.2000.3457, available online at http://www.idealibrary.com on IDEAL®

AEROACOUSTIC RESPONSE OF A SLIT-SHAPED DIAPHRAGM IN A PIPE AT LOW HELMHOLTZ NUMBER, 1: QUASI-STEADY RESULTS

G. C. J. Hofmans and R. J. J. Boot

Fluid Dynamics Laboratory, Faculty of Applied Physics, Eindhoven University of Technology, Postbus 513, 5600 *MB Eindhoven, The Netherlands*

P. P. J. M. Durrieu and Y. Auregan

*Laboratoire d'Acoustique, Université du Maine, Au. Olivier Messiaen BP*535, 72017 *Le Mans, France*

and

A. Hirschberg

Fluid Dynamics Laboratory, Faculty of Applied Physics, Cascade 2.24, *Eindhoven University of Technology, Postbus* 513, 5600 *MB Eindhoven, The Netherlands. E-mail: a.hirschberg@phys.tue.nl*

(*Received* 18 *October* 1999, *and in final form* 18 *October* 2000)

The aeroacoustic response of a diaphragm in a pipe is studied by means of an analytical model and experimental measurements. The study is restricted to quasi-two-dimensional diaphragms with a sharp-edged rectangular aperture at conditions for which the acoustic source region can be considered compact. The compactness of the source can be realized under two conditions: either a low Strouhal number and a jet Mach number of the order unity; or a low jet Mach number and a Strouhal number of order unity. In this paper, the focus is on the first case. The second case of low Mach number and Strouhal number of order unity is discussed in a companion paper. The results of a quasi-steady theory are compared with measurements of the reflection and transmission coefficients of a diaphragm. The theoretical model is based on Ronneberger's model for a step-wise expansion (D. Ronneberger 1967, *Acustica* **19**, 222–235) and Bechert's description of an orifice used as an anechoic pipe termination (Bechert 1980 *Journal of Sound and Vibration* **70**, 389–405). An important phenomenon associated with the flow through a diaphragm is the so-called vena contracta effect. This effect is analyzed theoretically as a function of diaphragm opening and jet Mach number by using analytical results for a Borda tube. This allows the use of the theory up to Mach numbers of unity in the free jet downstream of the diaphragm. It is shown that at low frequencies the model and the experimental results are in good agreement. Significant deviations appear only when the Strouhal number reaches unity.

1. INTRODUCTION

Diaphragms are common elements in pipe systems, either used as a constriction of the flow in a pipe or as an aperture to a Helmholtz resonator mounted in the pipe wall. In Figure 1, examples of such configurations are shown. Both configurations are commonly used in car mufflers to suppress resonances in the exhaust pipe. Although several experimental investigations into the effects of diaphragms have been carried out previously, a detailed

0022-460X/01/260035 + 22 $35.00/0

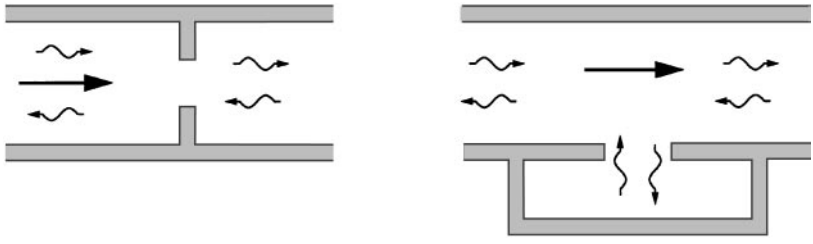

Figure 1. Configurations of a diaphragm in a pipe with a mean flow.

quantitative comparison of experimental and theoretical results is still lacking. In this paper, the focus is on the diaphragm acting as a strong constriction to the main pipe flow and experimental and theoretical results are compared. The influence of rapid changes in the pipe cross-section on the propagation of acoustic waves was observed already in the 19th century by Rayleigh [1]. Ingard [2] and Ingard and Ising [3] studied non-linear phenomena at large acoustic amplitudes associated with the acoustic flow through an orifice. But it was not until 1967 that Ronneberger [4] proposed a simple low-frequency theoretical description for the aeroacoustic effect of a subsonic mean flow through a stepwise expansion in a pipe taking into account effects due to mean-flow compressibility and associated variations in entropy. Bechert [5] followed by proposing a similar incompressible quasi-steady description for the effect of a subsonic mean flow through a diaphragm used as a pipe termination. He also provided an overview of the experimental work that was done until 1980. As an important result of his theoretical description Bechert found that for a certain mean flow Mach number the pipe termination is completely anechoic. This phenomenon has been discussed in terms of vortex-sound theory by Howe [6] and confirmed experimentally by Cummings and Eversman [7]. The theoretical work presented in this paper is an extension of the theories of Ronneberger and Bechert. It describes a diaphragm in a pipe, not just a diaphragm as a pipe termination, and it includes compressibility effects which had been neglected by Bechert. Another important phenomenon of the flow that is incorporated in the theoretical model is the so-called vena contracta effect. In other words, account is taken of the fact that flow separation at the diaphragm induces the formation of a jet flow which has a cross-sectional area smaller than the aperture of the diaphragm itself, as sketched in Figure 2. The idea to study the Mach-number dependence of this effect comes from preliminary studies of the acoustic response of diaphragms at high subsonic Mach numbers by Parchen and Bruggeman [8]. They could not explain their observations without assuming a Mach-number dependence of the vena contracta factor.

First, a quasi-steady acoustic model is presented for low-Mach-number flows. The acoustic effect of the diaphragm is studied by considering the acoustic pressure reflection and transmission coefficients. The model is extended by including compressibility effects. It is shown that, depending on the size of the aperture of the diaphragm relative to the pipe diameter, compressibility effects are important for an accurate modelling of the acoustic effects, even for quite low-Mach-number flows in the main pipe. The discussion on the vena contracta effect is based on an original analytical model for a Borda tube placed in the opening of the diaphragm. A general interpolation formula is presented which allows a calculation of the vena contracta factor from existing data and theories for the limit cases of a diaphragm in an infinite wall and of an incompressible flow. The discussion is restricted to diaphragms with sharp edges. The influence of both aperture geometry and Mach number on the vena contracta is discussed. Lastly, low frequency experiments on a slit-like

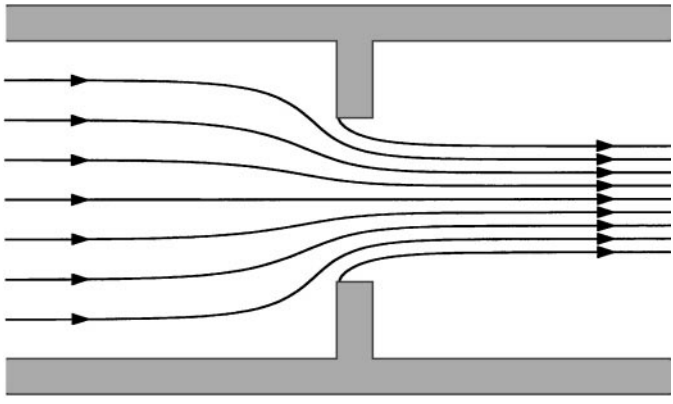

Figure 2. The vena contracta of the flow through a diaphragm.

diaphragm in a pipe are compared to the quasi-steady acoustic model. Data for circular apertures and perforated plates are provided by Durrieu *et al.* [9] in which also the design of an anechoic termination for a finite range of Mach numbers is considered.

2. QUASI-STEADY MODELLING

2.1. DEFINING THE APPROXIMATIONS

In this paper, two different models to determine the acoustic response of a diaphragm in a pipe are presented. The models represent different approximations of the flow through the diaphragm. A set of non-dimensional numbers is introduced in order to define the limits of validity of each model. In this section, the non-dimensional numbers are discussed and the various limits associated with these numbers for a slit-shaped diaphragm in a two-dimensional channel are explained. In subsequent sections the following non-dimensional numbers are used: $M_1 = u_1/c_1$, Mach number; $\mathrm{Sr} = f h_d/u_d$, Strouhal number; $\mathrm{He} = f h_p/c_1$ Helmholtz number; $\mathrm{Re} = u_1 h_p/\nu$, Reynolds number; $u_{ac} = u_1'/u_1$, acoustic amplitude; $\Upsilon = S_j/S_d$, vena contracta (contraction) ratio; $\mathscr{S} = S_p/S_j = S_p/\Upsilon S_d$, cross-sectional-area ratio. Here u_1 and c_1 are the steady main flow velocity and the speed of sound in the pipe upstream of the diaphragm respectively. f is the frequency of the acoustic waves, h_d is the height of the aperture of the (two-dimensional, slit-shaped) diaphragm $u_d = (S_p/S_d)u_1$ is the average velocity across the aperture of the diaphragm in the incompressible approximation, h_p is the height of the pipe (when it is considered as a two-dimensional channel), ν is the kinematic viscosity, u_1' is the acoustic velocity in the plane-wave region of the pipe upstream of the diaphragm, S_j is the cross-sectional area of the jet, S_d is the cross-sectional area of the aperture of the diaphragm, and S_p is the cross-sectional area of the pipe. The cross-sectional area is defined as the height h_p times the width W of the pipe: e.g., $S_p = (W h_p)$. Some of these quantities are shown in Figure 3.

The flow through a diaphragm (sketched in Figure 3) can be separated into three regions: first, the uniform flow in the upstream pipe segment in which plane acoustic waves are travelling in upstream and downstream directions; second, the compact flow in the acoustic source region around the diaphragm where acoustic energy is produced or dissipated; and third, the uniform flow in the downstream pipe segment in which again plane acoustic waves are travelling in upstream and downstream directions. The Strouhal number, as

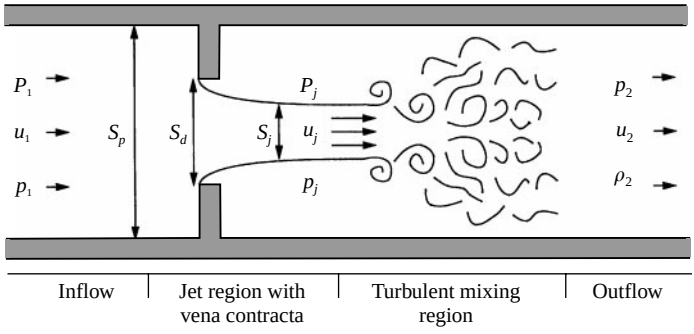

Figure 3. Schematic drawing of a steady flow through a diaphragm in a pipe with a mean flow. A uniform inflow is accelerated through the diaphragm into the jet. The turbulent jet is followed by the turbulent mixing region which results in the uniform outflow.

defined above, is a measure of the importance of unsteady flow effects in the source region. A low value indicates that the jet flow can be considered quasi-steady while a high value indicates an essentially unsteady jet flow. The Helmholtz number is a measure for the size of the source region relative to the wavelength of the acoustic wave. When He approaches zero the wavelength of the acoustic wave is much larger than the linear dimension of the source region. In that case the phase difference of acoustic quantities across the source region can be neglected and the source region is called compact. In this paper, the focus is on low-frequency acoustic waves only, i.e., the source region can be considered compact.

Although seven non-dimensional numbers have been defined, only five of these numbers can be chosen independently. Therefore, when the Strouhal number and the Helmholtz numbers are chosen as independent numbers, the Mach number M_1 is related to He and Sr by $M_1 = (S_d/S_p)^2$ (He/Sr). M_1 is a measure of the importance of convective effects on the acoustic wave propagation in the pipe. The limit of He $\to 0$ (while keeping Sr fixed) produces the limit $M_1 \to 0$: consequently, an essentially unsteady but incompressible description of the source region can be used. The limit of Sr $\to \infty$ (while keeping He constant) also produces the limit $M_1 \to 0$: consequently, the convection effects and compressibility effects in the source region are negligible and the description of the source region is essentially unsteady. This last limit corresponds in a linear approximation to the classical acoustic behavior in a stagnant fluid. In that case, the potential-flow approximation is actually recovered because the convection velocity u_1 is negligible in wave propagation and in the flow through the diaphragm. Although both cases correspond to low Mach numbers, they are to be considered as approaching this limit from different directions and as such both descriptions can be very different [10]. For subsonic flows the Mach number in the jet M_j can be approximated by the product of the cross-sectional-area ratio $\mathscr{S}$ and M_1. This is a measure of the importance of compressibility in the source region: when $M_j^2 \ll 1$ and He $\ll 1$ the source region can be considered incompressible and compact.

In this paper, the focus is on high Reynolds number flow ($\mathscr{O}(10^5)$), which means that the effect of viscosity is restricted to thin boundary layers. Upstream of the diaphragm an inviscid flow description can be used. However, one important viscous effect is taken into account: flow separation at the edges of the diaphragm. While the jet flow is also frictionless, turbulent dissipation is assumed between the jet flow and the one-dimensional flow region downstream of the diaphragm. Only separation at sharp edges (meaning fixed separation points even in an unsteady flow) is considered. Furthermore, only a compact source region is considered, so He $\ll 1$. The first limit that is treated is Sr $\ll 1$ such that also $M_1 \ll 1$. In that case the quasi-steady incompressible-flow model of the next paragraph can be used. In the

case of the limit of $\mathrm{Sr} \ll 1$ such that M_1 is finite, compressibility in the source region is essential. In that case the quasi-steady compressible flow model of the subsequent section can be used. The third limit that is treated is Sr finite such that $M_1 \ll 1$. In that case the unsteady numerical incompressible-flow model presented in a companion paper [11] can be used.

2.2. INCOMPRESSIBLE-FLOW MODEL

An incompressible quasi-steady flow model of the acoustic response of a flow through a diaphragm in a pipe is presented. The effect of the diaphragm on the acoustic flow is reduced to a discontinuity in the acoustic pressure across the diaphragm. If the magnitude of this pressure discontinuity is proportional to the acoustic amplitude, the effect of the diaphragm on the acoustic flow can be described by the scattering matrix: a set of linear equations relating the acoustic pressure downstream of the diaphragm to the acoustic pressure upstream of the diaphragm. Due to the assumption of a locally incompressible flow, this model is valid only for low-Mach-number flows with a compact source region. It is important to recall that the jet velocity can be much higher than the velocity in the pipe but in the first approximation considered here it has to be much less than the speed of sound.

In Figure 3, a schematic representation of the flow is shown. A uniform flow is forced through a diaphragm resulting in the jet flow. Because of the sharp edges of the diaphragm the jet will exhibit the so-called vena contracta effect: the jet will contract further than the aperture of the diaphragm (see section 3 for an extensive discussion). Within the jet the flow is isentropic and irrotational so that Bernoulli's equation can be applied together with the continuity equation:

$$S_p u_1 = S_j u_j, \qquad p_1 + \tfrac{1}{2}\rho_0 u_1^2 = p_j + \tfrac{1}{2}\rho_0 u_j^2. \tag{1, 2}$$

The velocity outside the jet flow is assumed to be negligibly small and at the end of the jet the pressure is assumed to be uniform over the pipe cross-section. Further downstream, the jet flow becomes turbulent and its structure is destroyed in the turbulent mixing region. This region results in a uniform flow in the pipe downstream of the mixing region.

The description of the flow up to the jet flow is identical to the description by Bechert [5] of the flow through a diaphragm used as a pipe termination. However, the boundary condition of zero pressure recovery in the turbulent mixing region in free space that is used by Bechert is replaced by a model that relates the quantities across the turbulent mixing region. In the turbulent mixing region a pressure recovery takes place. Friction is essential in the bulk of this region. The flow is assumed to be adiabatic but no longer isentropic. Integral formulations of the steady continuity and momentum equations are applied to this region to describe this behavior:

$$S_j u_j = S_p u_2, \qquad S_p p_j + S_j \rho_0 u_j^2 = S_p p_2 + S_p \rho_0 u_2^2. \tag{3, 4}$$

Here in the mixing region friction at the walls is neglected. In these equations the density ρ_0 is constant. It is straightforward to rewrite the equations in a form relating the pressure p_1 at the inflow to the pressure p_2 at the outflow. This results in an equation similar to Bechert's equation for a pipe termination:

$$p_1 - p_2 = \tfrac{1}{2}\rho_0 u_1^2 \left(\frac{S_p}{S_j} - 1 \right)^2. \tag{5}$$

Compared to Bechert's result for a pipe termination the pressure loss $(p_2 - p_j)$ is reduced: which is due to the pressure recovery in the turbulent mixing region:

$$p_2 - p_j = \rho_0 u_1^2 \left(\frac{S_p}{S_j} - 1 \right). \tag{6}$$

In order to determine the acoustic effect of the diaphragm acoustic perturbations p_i' are introduced to describe the oscillation of the pressure p around a mean value p_i:

$$p = p_i + p_i'. \tag{7}$$

The same is done for the velocity:

$$u = u_i + u_i'. \tag{8}$$

The equations are linearized in p_i' and u_i'. Here p_i and u_i are the steady flow quantities obtained by solving equations (1)–(4) for the steady flow ($p_i' = 0$, $u_i' = 0$). The acoustic pressure perturbations can be split into downstream travelling waves p_i^+ and upstream travelling waves p_i^- so that

$$p_i' = p_i^+ + p_i^-. \tag{9}$$

Then the acoustic velocity perturbations in the pipe are related to the acoustic pressure perturbations by

$$u_i' = p_i^+ / \rho_0 c_0 - p_i^- / \rho_0 c_0 \tag{10}$$

with c_0 being the speed of sound. The acoustic perturbations satisfy the linearized version of equation (5) and of the mass conservation equations (1) and (3):

$$p_1^+ - p_1^- = p_2^+ - p_2^-, \tag{11}$$

$$p_1^+ + p_1^- - (p_2^+ + p_2^-) = M_1 \left(\frac{S_p}{S_j} - 1 \right)^2 (p_1^+ - p_1^-). \tag{12}$$

Here $M_1 = u_1/c_0$ is the Mach number of the steady flow in the pipe. These equations can be rewritten in terms of a scattering matrix [12]:

$$\begin{pmatrix} p_2^+ \\ p_1^- \end{pmatrix} = \begin{pmatrix} T^+ R^- \\ R^+ T^- \end{pmatrix} \begin{pmatrix} p_1^+ \\ p_2^- \end{pmatrix}. \tag{13}$$

This notation is very useful because it relates the outgoing waves (away from the diaphragm) to the incoming waves (towards the diaphragm) by means of reflection and transmission coefficients. In a linear system the outgoing wave p_1^- is the result of the reflection $R^+ p_1^+$ of the incoming wave p_1^+ from the left and the transmission $T^- p_2^-$ of the incoming wave p_2^- from the right. A similar relationship holds for the outgoing wave p_2^+. Rewriting equations (11) and (12) in the form of equation (13) yields

$$\begin{pmatrix} p_2^+ \\ p_1^- \end{pmatrix} = \frac{1}{2 + M_1 \beta} \begin{pmatrix} 2 & M_1 \beta \\ M_1 \beta & 2 \end{pmatrix} \begin{pmatrix} p_1^+ \\ p_2^- \end{pmatrix}, \tag{14}$$

where $\beta = (S_p/S_j - 1)^2$ represents the combined influence of the geometry and the vena contracta effect. The vena contracta factor $\Upsilon = S_j/S_d$ will be discussed in section 3. The

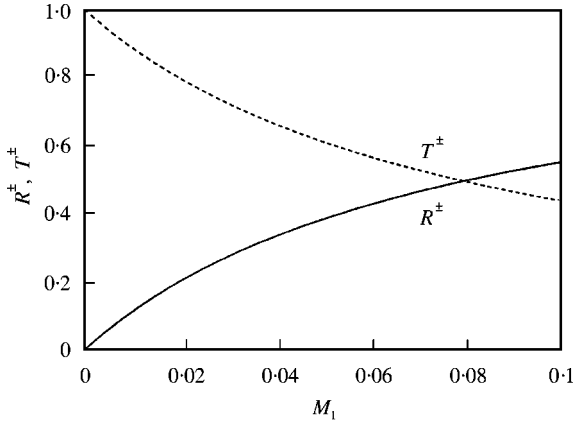

Figure 4. Scattering-matrix elements $R^{\pm}$ and $T^{\pm}$ as defined by equation (14) as a function of Mach number M_1. The value of $\beta = ((S_p/S_j) - 1)^2$ is 25 so for $M_1 = 0{\cdot}1$ compressibility is already important since $M_j = u_j/c_0 = 0{\cdot}6$.

matrix is symmetric and the elements satisfy the relationship $R^+ + T^+ = R^- + T^- = 1$. This property is a result of the incompressibility of the flow model.

In Figure 4, the elements of the scattering matrix are presented as a function of the Mach number M_1 in the pipe. The value of β used in this figure is 25 which means that $S_p/S_j = 6$. This implies quite a strong constriction in the pipe and already at a Mach number of 0·05 in the main pipe (so a Mach number of 0·3 in the jet) compressibility becomes significant. When the Mach number is reduced to zero while keeping Sr fixed at a small value such that $\mathrm{Sr} \ll 1$ the influence of the diaphragm in the quasi-steady model disappears; hence $R^{\pm} = 0$ and $T^{\pm} = 1$.

Equation (14) is valid when convection effects are neglected in the regions of acoustic wave propagation. In case these effects cannot be neglected but the source region can still be considered incompressible, then the pressure perturbations should be replaced by total-exergy perturbations:† $p_i^{\pm} \rightarrow p_i^{\pm}(1 \pm M_i)$. In the next section, the compressible-flow model is discussed and it is shown that in that case the total-exergy perturbations are a natural choice of variables.

2.3. COMPRESSIBLE-FLOW MODEL

When increasing the Mach number of the flow the compressibility has an important effect on the acoustic response of a diaphragm in a pipe. For example, at certain conditions the Mach number in the jet region reaches unity and this restricts the mass flow and cuts off the exchange of acoustic information across the diaphragm from the downstream to the upstream side. In the present study, subsonic flows are considered where the jet Mach number is at most equal to unity. As in the previous section, one can derive a quasi-steady compressible-flow model to describe the acoustic response of a diaphragm in a pipe. A compressible quasi-steady flow model has the same restrictions as the incompressible-flow model, i.e., the source region must be compact (small Helmholtz number) and the Strouhal number must be low. The model is based on the compressible low-frequency flow model for the acoustic response of a step-wise expansion in a pipe as

†Total-exergy fluctuations are defined as $B_i^{\pm} = (p_i^{\pm}/\rho_i)(1 \pm M_i)$ upon neglecting entropy fluctuations. This corresponds to the total-enthalpy fluctuations as defined by Doak [13] and Howe [14]. As long as entropy fluctuations are neglected there is no distinction between exergy and enthalpy.

presented by Ronneberger [1]. Ronneberger introduced the concept of entropy waves of Kovasznay [15] in his model. These are entropy changes that are convected with the main flow velocity. In the present model a new scattering matrix in terms of the total exergy is introduced that also relates the incoming entropy wave σ_1 to the outgoing entropy wave σ_2:

$$\begin{pmatrix} (1+M_2)p_2^+ \\ (1-M_1)p_1^- \\ \sigma_2 \end{pmatrix} = \begin{pmatrix} S_{11} & S_{12} & S_{13} \\ S_{21} & S_{22} & S_{23} \\ S_{31} & S_{32} & S_{33} \end{pmatrix} \begin{pmatrix} (1+M_1)p_1^+ \\ (1-M_2)p_2^- \\ \sigma_1 \end{pmatrix}. \tag{15}$$

When a homentropic flow is assumed upstream of the diaphragm the incoming entropy wave vanishes ($\sigma_1 = 0$). The scattering matrix can then be reduced to a form similar to equation (13) but now for the total-exergy waves

$$\begin{pmatrix} (1+M_2)p_2^+ \\ (1-M_1)p_1^- \end{pmatrix} = \begin{pmatrix} T^+ R^- \\ R^+ T^- \end{pmatrix} \begin{pmatrix} (1+M_1)p_1^+ \\ (1-M_2)p_2^- \end{pmatrix}. \tag{16}$$

In Figure 3, a schematic representation of the flow is shown. Since now the density is a variable one needs six equations to describe the low-frequency acoustic response of a diaphragm. The set of four equations of the steady incompressible-flow model is modified and completed by the isentropic gas relation applied to the inflow region up to the jet and the integral formulation of the energy equation that states that energy is conserved in the flow because heat transfer at the walls is neglected. A perfect gas with constant specific heats is assumed! Neglecting heat transfer and friction at the walls one finds

$$S_p \rho_1 u_1 = S_j \rho_j u_j, \qquad S_j \rho_j u_j = S_p \rho_2 u_2, \tag{17, 18}$$

$$\tfrac{1}{2}u_1^2 + \frac{\gamma}{\gamma-1}\frac{p_1}{\rho_1} = \tfrac{1}{2}u_j^2 + \frac{\gamma}{\gamma-1}\frac{p_j}{\rho_j}, \tag{19}$$

$$S_p p_j + S_j \rho_j u_j^2 = S_p p_2 + S_p \rho_2 u_2^2, \qquad p_1/p_j = (\rho_1/\rho_j)^\gamma, \tag{20, 21}$$

$$\tfrac{1}{2}u_1^2 + \frac{\gamma}{\gamma-1}\frac{p_1}{\rho_1} = \tfrac{1}{2}u_2^2 + \frac{\gamma}{\gamma-1}\frac{p_2}{\rho_2}, \tag{22}$$

where γ is the ratio of specific heats at constant pressure and volume. The energy equation in that case is equivalent to the conservation of total enthalpy:‡ $B_1 = B_2$. As in the incompressible model wall friction has been neglected in equation (20) and heat transfer in equation (22), which implicitly corresponds to the assumption of a short mixing region downstream of the jet.

In order to find the elements of the scattering matrix (15) the equations are split into a set of non-linear equations for the steady flow and a set of linearized equations for the acoustic perturbations. The elements S_{ij} of the scattering matrix contain only steady flow information. So, first the non-linear equations for the steady main flow have to be solved. The procedure is as follows. Equations (17, 19, 21) together with $c^2 = \gamma p/\rho$ yield an equation that relates M_1 to the density ratio $\wp_{1j} = \rho_1/\rho_j$,

$$M_1 = \sqrt{\frac{2}{\gamma-1}}\sqrt{\frac{1-\wp_{1j}^{1-\gamma}}{\mathscr{S}^2\wp_{1j}^2 - 1}}, \tag{23}$$

‡For a calorically perfect gas the total enthalpy is $B = C_p T + \frac{1}{2}u^2 = \gamma/(\gamma-1)p/\rho + \frac{1}{2}u^2$.

where $\mathscr{S} = S_p/S_j = S_p/(\Upsilon S_d)$ includes the vena contracta effect: which, as will be seen in section 3, is a function of the Mach number. Given the Mach number in the pipe M_1 and assuming $\mathscr{S}$ to be determined as well, equation (23) yields the density ratio $\wp_{1j}$. Then the jet Mach number is obtained as

$$M_j = M_1 \mathscr{S} \wp_{1j}^{(\gamma+1)/2}. \tag{24}$$

The momentum equation (20) applied across the turbulent mixing region results in

$$p_j(1 + \gamma \mathscr{S}^{-1} M_j^2) = p_2(1 + \gamma M_2^2).$$

Since $p_2/p_j = (p_2/\rho_2)(\rho_2/\rho_j)(\rho_j/p_j)$ and from mass conservation (18) $\rho_2/\rho_j = \mathscr{S}^{-1} u_j/u_2 = \mathscr{S}^{-1}(M_j/M_2)(c_j/c_2)$ this equation can be rewritten as

$$\frac{c_2}{c_j} = \frac{\mathscr{S} M_2}{M_j} \frac{(1 + \gamma \mathscr{S}^{-1} M_j^2)}{(1 + \gamma M_2^2)}. \tag{25}$$

Together with the energy equation (22) and Bernoulli's equation (19),

$$\frac{\gamma - 1}{2} M_j^2 + 1 = \frac{c_2^2}{c_j^2} \left(\frac{\gamma - 1}{2} M_2^2 + 1 \right), \tag{26}$$

this results in a quadratic equation for M_2^2. Now both M_2 and $\wp_{2j}$ can be obtained as functions of M_j. When the dependency of $\mathscr{S}$ on M_j has to be taken into account the procedure described above is repeated iteratively by calculating a new value of $\mathscr{S}$ after each iteration (substitution method).

Given M_1, all other parameters $\mathscr{S}$, $\wp_{1j}$ (equation (23)), M_j (equation (24)), M_2 (equation (26)) and $\wp_{12} = \wp_{1j}/\wp_{2j}$ can be obtained. In a similar way as for the incompressible case, acoustic perturbations are introduced and the equations are linearized. This yields expressions for the coefficients S_{ij} of the scattering matrix as a function of mean flow parameters. Since the elements S_{ij} of the scattering matrix (15) can be written as functions of these variables, the scattering matrix is hereby known. However, these functions are too complex to be presented here.

3. VENA CONTRACTA

An important parameter for the aeroacoustic response of a diaphragm is the ratio of the velocity in the jet and the velocity in the pipe. The jet velocity is determined by the aperture of the diaphragm combined with the so-called vena contracta effect. The flow separates at a sharp corner in the direction of the local grazing flow along the wall. Just upstream of the sharp edges of the diaphragm the flow is directed towards the pipe axis. To pass through the diaphragm the flow has to bend in the direction of the axis of the main pipe. This results in an additional contraction of the flow after flow separation at the edges of the diaphragm. In Figure 5, this effect is illustrated. The contraction ratio Υ is defined as the ratio of the jet cross-section S_j and the diaphragm cross-section S_d. For the two-dimensional flow considered here, this is equal to the ratio of the heights $\Upsilon = y_j/y_d$.

A value for the contraction ratio of the flow through a diaphragm was calculated by Kirchhoff for a two-dimensional incompressible flow through a slit in an infinitely exteneded thin plate (as shown on the left in Figure 5). He found the value $\Upsilon_0 = \pi/(\pi + 2) \approx 0{\cdot}611$ (see reference [16]).

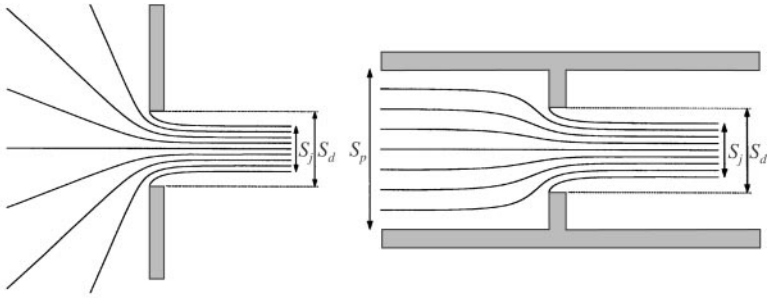

Figure 5. Streamlines of the two-dimensional incompressible flow through a diaphragm. Shown on the left is the flow through a hole in a flat plate and on the right the flow through a diaphragm in a pipe.

Even for perfectly sharp edges of the diaphragm there are a number of reasons why the value of the contraction ratio is different from the value found by Kirchhoff. The most important one is the influence of the geometry as determined by the ratio of the area of the diaphragm opening to the pipe cross-sectional area. Another significant influence is due to the compressibility of the flow. As indicated by Blevins [17], the influence of the Reynolds number also becomes important when the Reynolds number is much smaller than 10^4. Based on the expression for circular diaphragms in cylindrical pipes presented by Blevins, the influence of the Reynolds number is expected to be small in our experiments and is therefore neglected in our analysis. Finally, the sharpness of the edges of the diaphragm is crucial. Blevins presented data that show that rounding the edges by a few percent of the height of the opening reduces the vena contracta effect almost completely. In our experiments, considerable attention was given to keeping the rounding of the edges within 1% of the diaphragm height y_d and in the further analysis sharp edges are assumed. In this section, the focus is on the influence of the geometrical parameter S_d/S_p and the influence of the compressibility; i.e., the Mach number M_j. In this case $\Upsilon = S_j/S_d$ is a function $\Upsilon(S_d/S_p, M_j)$ of both the surface-area ratio S_d/S_p and the jet Mach number M_j.

The Borda mouthpiece is a configuration for which a simple analytical equation can be derived that determines the contraction ratio Υ as a function of both Mach number and surface area ratio. In its original configuration the Borda mouthpiece is a long narrow tube that extends into a large vessel as shown in Figure 6 [16]. Here such a Borda tube is considered to be placed in the opening of a diaphragm in a pipe. It is assumed that the length of the Borda tube is large compared to its diameter. In that case it is possible to apply a momentum balance in the x-direction along the boundary shown in Figure 6 (see also reference [18]) in which stagnation of the flow is assumed at the upstream wall of the diaphragm.

On the left of the configuration a uniform inflow condition is assumed: velocity u_1, pressure p_1, and density ρ_1. On the right, along the upstream walls of the diaphragm, a stagnation condition is assumed so that the velocity is equal to zero and the pressure is equal to the upstream stagnation pressure p_0. The jet flow at the position of the diaphragm is also assumed to be uniform: velocity u_j, pressure p_j, and density ρ_j. Furthermore, the acceleration of the fluid from the pipe into the jet is assumed to be isentropic. Then mass conservation $S_p\rho_1 u_1 = S_j\rho_j u_j$ together with the isentropic relation $p_1/p_j = (\rho_1/\rho_j)^\gamma$ and $c^2 = \gamma p/\rho$ yields the equation

$$\Upsilon \frac{S_d}{S_p} = \frac{M_1}{M_j}\left(\frac{\rho_1}{\rho_j}\right)^{(\gamma+1)/2}. \tag{27}$$

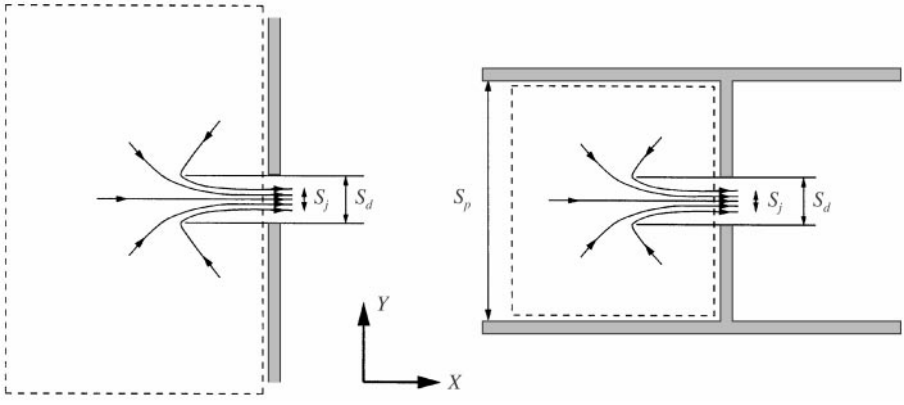

Figure 6. Borda mouthpiece (left) and Borda mouthpiece in a vessel (right).

The integral form of the momentum balance applied in the x-direction to the control surface defined in Figure 6 results in

$$S_p(p_1 + \rho_1 u_1^2) = (S_p - S_d)p_0 + S_d p_j + S_j \rho_j u_2^2,$$

which after division by $S_p p_1$ can be rewritten as

$$1 + \gamma M_1^2 = \left(1 - \frac{S_d}{S_p}\right)\frac{p_0}{p_1} + \frac{S_d}{S_p}(1 + \Upsilon\gamma M_j^2)\frac{p_j}{p_1}. \tag{28}$$

The pressure ratios can be expressed in terms of Mach numbers by using the compressible form of Bernoulli's equation:

$$\frac{p_0}{p_1} = (\tfrac{1}{2}(\gamma - 1)M_1^2 + 1)^{\gamma/(\gamma-1)}, \tag{29}$$

$$\frac{p_j}{p_1} = \left(\frac{\rho_j}{\rho_1}\right)^{\gamma} = \left(\frac{\tfrac{1}{2}(\gamma - 1)M_1^2 + 1}{\tfrac{1}{2}(\gamma - 1)M_j^2 + 1}\right)^{\gamma/(\gamma-1)}. \tag{30}$$

When S_d/S_p and M_j are used as input parameters, substitution of these equations in equation (28) results in an implicit equation for M_1:

$$1 + \gamma M_1^2 = \left(1 - \frac{S_d}{S_p}\right)(\tfrac{1}{2}(\gamma - 1)M_1^2 + 1)^{\gamma/(\gamma-1)} + \frac{S_d}{S_p}\left(\frac{\tfrac{1}{2}(\gamma - 1)M_1^2 + 1}{\tfrac{1}{2}(\gamma - 1)M_j^2 + 1}\right)^{\gamma/(\gamma-1)} + \gamma M_j M_1 \left(\frac{\tfrac{1}{2}(\gamma - 1)M_1^2 + 1}{\tfrac{1}{2}(\gamma - 1)M_j^2 + 1}\right)^{1/2}. \tag{31}$$

The value of M_1 is obtained by solving iteratively this implicit equation and the corresponding Υ is obtained after substitution of the result into equation (27).

In Figure 7, the contraction ratio Υ is shown as a function of jet Mach number for five different values of S_d/S_p. By comparing the different curves one finds that the effect of compressibility is not sensitive to the geometric parameter S_d/S_p. For S_d/S_p less than 0·6 the different curves can be approximated accurately by just shifting the curve for $S_d/S_p = 0$

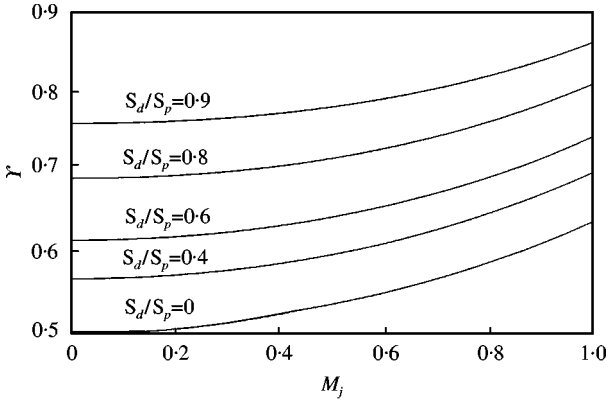

Figure 7. Contraction ratio $\Upsilon = S_j/S_d$ as a function of jet Mach number M_j for five different values of the ratio S_d/S_p.

upwards. An accurate approximation for Υ for $S_d/S_p < 0{\cdot}6$ therefore is

$$\Upsilon(S_d/S_p, M_j) \approx \Upsilon(S_d/S_p, 0) + \Upsilon(0, M_j) - \Upsilon(0, 0), \tag{32}$$

in which

$$\Upsilon(S_d/S_p, 0) = \frac{1}{1 + \sqrt{1 - S_d/S_p}}, \quad \Upsilon(0, M_j) = \frac{(1 + (\gamma - 1)/2\,M_j^2)^{\gamma/(\gamma - 1)} - 1}{\gamma M_j^2}$$

and $\Upsilon(0, 0) = 1/2$.

For $S_d/S_p < 0{\cdot}6$ this expression results in an approximate value for Υ that is within 0·5% of the exact solution. So the most important influence of the geometric parameter is that it determines the offset of Υ for $M_j = 0$. The effect of the compressibility is then almost independent of the geometry. Since this geometry bears a strong resemblance to the geometry of a thin diaphragm in a pipe one expects that a similar behavior applies to that case. Thus, one can restrict oneself to deriving $\Upsilon(S_d/S_p, 0)$ and $\Upsilon(0, M_j)$ for the case of a diaphragm in a pipe. One can then use the interpolation formula (32) to calculate $\Upsilon(S_d/S_p, M_j)$.

By means of a hodograph method Busemann [9] derived an expression for the contraction ratio $\Upsilon_0 = (S_d/S_p, 0)$ of a two-dimensional pipe flow through a diaphragm. The hodograph method (see reference [16]) consists in constructing a flow solution in the velocity plane which is subsequently transformed to the physical plane by integrating along the stream lines.[§] The geometry that was considered by Busemann is shown on the right in Figure 5. A diaphragm with an opening of S_d is placed in a pipe of height S_p. Behind the diaphragm the flow forms a jet with height S_j. The contraction ratio Υ_0 derived by Busemann is the solution of the implicit equation

$$\Upsilon_0 = \frac{S_j}{S_d} = \frac{\pi}{\pi + 2((1/\Upsilon_0)\,S_p/S_d - \Upsilon_0 S_d/S_p)\arctan(\Upsilon_0 S_d/S_p)}. \tag{33}$$

In this equation, the asymptotic solution of Kirchhoff can be found by taking the limit of $S_d \ll S_p$. In Figure 8, the contraction ratio Υ is shown as a function of the ratio S_d/S_p. The two limits of the solution are $\Upsilon_0 = \pi/(\pi + 2)$ for $S_d/S_p = 0$ and $\Upsilon_0 = 1$ for $S_d/S_p = 1$. It is

[§]In two-dimensional potential-flow theory the complex velocity $w = u + \mathrm{i}v$ is related to the complex stream function F by: $\bar{w} = \mathrm{d}F(z)/\mathrm{d}z$ where $z = x + \mathrm{i}y$. When it is possible to construct $F(w)$ the physical co-ordinates z can be obtained by integration: $z = \int \mathrm{d}F/\bar{w} + \text{constant}$.

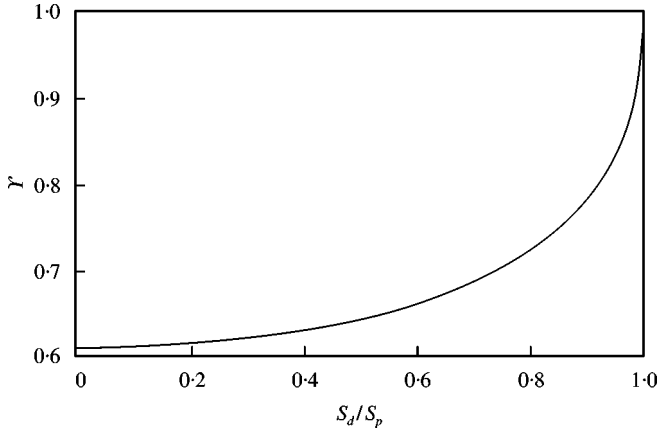

Figure 8. Contraction ratio $\Upsilon(S_d/S_p, 0)$ as a function of the ratio of diaphragm opening and pipe height [19].

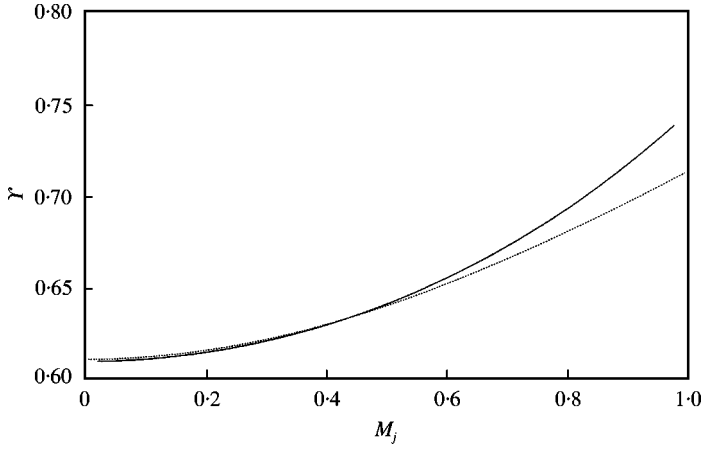

Figure 9. Contraction ratio $\Upsilon(0, M_j)$ as a function of Mach number M_j in the jet for a hole in a flat plate. Solution obtained by Chaplygin [18]; ——, Tangent gas (Shapiro); ——, Chaplygin.

clear from Figure 8 that for $S_d/S_p \leqslant 0{\cdot}2$ Kirchhoff's result is a very reasonable approximation.

Chaplygin derived an exact solution for a two-dimensional compressible flow through a hole in an infinitely extended thin plate by means of the hodograph method [18]. Since this solution is a rather complex expression containing hypergeometric functions, the solution is presented in Figure 9.

With Busemann's solution $\Upsilon(S_d/S_p, 0)$ for $M_j = 0$, Chaplygin's solution $\Upsilon(0, M_j)$ for $S_d/S_p = 0$, and Kirchhoff's solution $\Upsilon(0, 0) = \Upsilon_0 = \pi/(\pi + 2)$, one can apply equation (32) to the case of the diaphragm in a pipe and thus find an approximation for $\Upsilon(S_d/S_p, M_j)$.

4. COMPRESSIBLE SCATTERING MATRIX

The elements of the 2×2 compressible scattering matrix of equation (16) with a constant value of $\mathscr{S}$ are compared to the elements of the equivalent matrix in the incompressible case in Figure 10. For low Mach number the incompressible-flow model and the

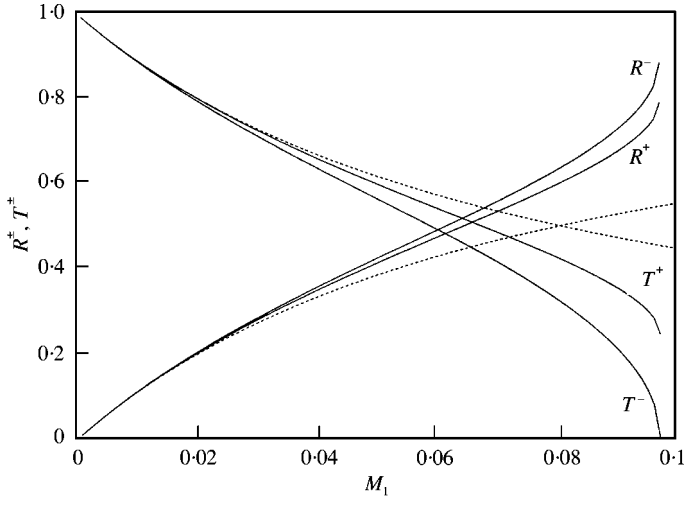

Figure 10. Scattering-matrix elements $R^{\pm}$ and $T^{\pm}$ as defined by equation (16) as a function of Mach number M_1 compared to the incompressible flow results for the case where $\mathscr{S} = S_p/S_j = 5{\cdot}97$. The incompressible flow results are given by the dashed lines.

compressible-flow model agree. It can be shown that the matrix elements in the limit of very low Mach number are equal to the elements of the incompressible scattering matrix (14). This also indicates that the scattering matrix (even in the incompressible case) should be considered a scattering matrix for total-exergy waves. It is clearly evident from Figure 10 that T^+ diverges from T^- (as well as R^+ from R^-) as the Mach number increases. So the symmetry of the scattering matrix is lost. Another property of the incompressible flow model is lost: T^+ and R^+ do not add up to one and the same holds for T^- and R^-. At a Mach number close to 0·1 the flow in the jet becomes sonic. In that case, no information can travel upstream through the diaphragm and therefore $T^- = 0$. This restriction does not apply to information that travels downstream through the diaphragm so T^+ is not equal to zero. This already explains the asymmetry between the behavior of T^+ and that of T^-. Note that in the discussion of the incompressible scattering matrix it was implicitly assumed that the effect of the vena contracta factor S_j/S_d was known and fixed, independent of the Mach number. As was seen in the previous paragraph there is an additional implicit dependence on the Mach number M_j through the variation of $\mathscr{S}$ as a function of M_j in the case of a compressible scattering matrix.

5. EXPERIMENTAL RESULTS

5.1. EXPERIMENTAL SET-UP AND PROCEDURE

In order to verify the accuracy of the models introduced in the previous sections, low-frequency experiments have been performed on the acoustic behavior of a diaphragm in a pipe. The focus was on the measurement of the Mach-number dependence at low frequency. In Figure 11, a schematic drawing of the set-up is presented. This is essentially the same set-up as used earlier by Peters [20]. Dry air at high pressure enters the system at (A). The flow is controlled by the reduction valve and the flow rate is measured at (C). The mean static pressure (accuracy 0·1%) and temperature (accuracy 0·1%) are measured in order to characterize the conditions of the experiments. From these data the speed of sound

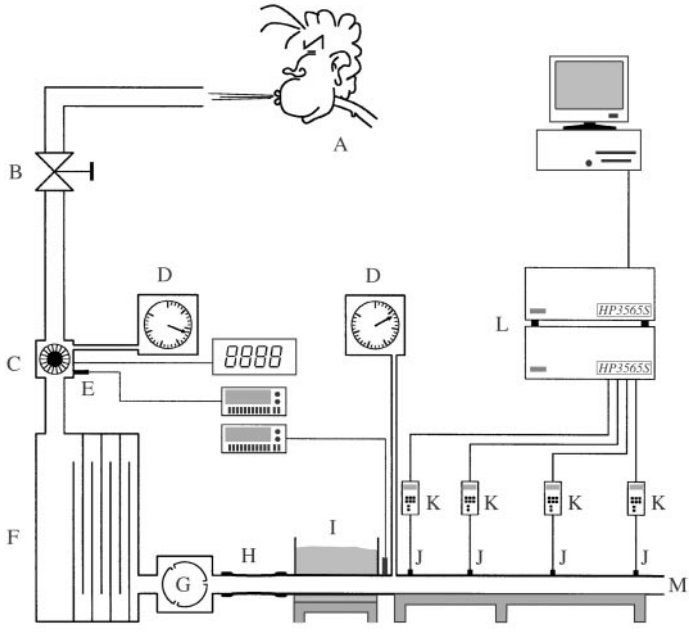

Figure 11. Experimental set-sup: (A) high-pressure supply, (B) pressure reduction valve, (C) flow meter, (D) manometer, (E) thermometer, (F) settling chamber, (G) siren, (H) flexible connection, (I) sand box, (J) piezo-electric pressure transducers, (K) charge amplifiers, (L) data analyzer, (M) pipe termination.

c_1 is determined which together with the flow rate provides the Mach number M_1 of the flow (accuracy 2%). In the following discussion of the experiments the index 1 will often be omitted and will be referred to as the Mach number of the experiments. Please note, however, that account has been taken of the difference between the upstream Mach number M_1 and the downstream Mach number M_2 in the analysis of the acoustical data. After passing the settling chamber the flow is led through the sound source: a siren. Here amplitude and frequency of the acoustic perturbations can be adjusted. Via a flexible connection tube and a box of sand for damping mechanical vibrations the flow finally enters the test section. This is a 6 m long cylindrical pipe with an internal radius of 15·013 mm and a wall thickness of 5 mm. The roughness of the internal walls of the pipe is of the order of 0·1 μm. The diaphragm is positioned at about 4 m downstream of the siren, which guarantees a fully developed turbulent pipe flow. At both sides of the diaphragm, piezo-electric pressure transducers (PCB 116A) are mounted in the pipe wall. The signals of the transducers are led to a set of charge amplifiers (Kistler 5011) which are connected to the data analyzer (HP-35650).

The reflection and transmission coefficients are measured by using the so-called two-microphone method described by Abom and Bodén [21]. Several pairs of microphones are used to measure the acoustic response of the diaphragm. The microphone positions are chosen for an optimal measurement. One microphone is at a pressure node while the other is close to a pressure anti-node of the standing wave pattern. This choice imposes a fixed frequency during the experiments. By using the data analyzer the complex transfer function $H_{ij}(\omega)$ is measured. This function is the ratio of the complex acoustic pressure amplitudes at positions x_i and x_j:

$$H_{ij}(\omega) = p'(x_i, \omega)/p'(x_j, \omega). \tag{34}$$

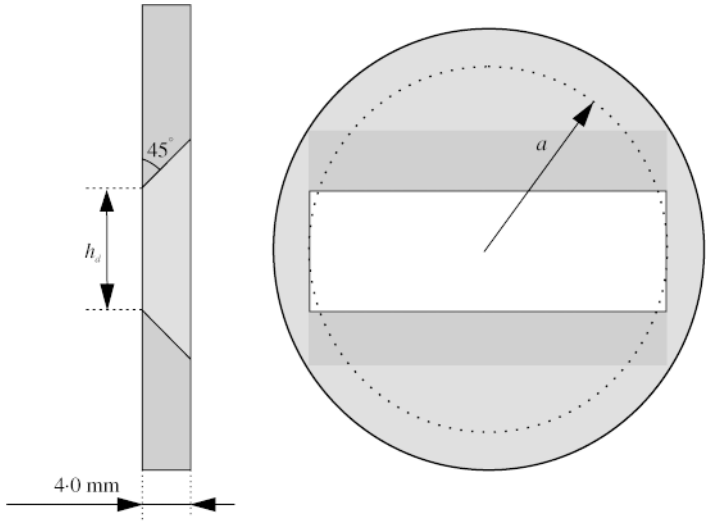

Figure 12. Three different slit-like diaphragms that have been used in the experiments: diaphragm I had $h_d = 10{\cdot}7$ mm and $S_d/S_p = 0{\cdot}45$; diaphragm II has $h_d = 6{\cdot}4$ mm and $S_d/S_p = 0{\cdot}27$; diaphragm III has $h_d = 2{\cdot}6$ mm and $S_d/S_p = 0{\cdot}11$.

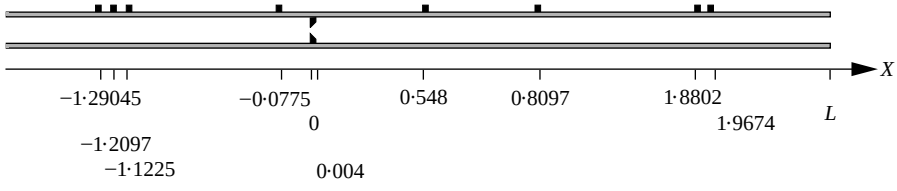

Figure 13. Microphone configuration used for the low-frequency measurements at 77 Hz. Positions of the microphones ■ given in meters.

The reflection and transmission coefficients can then be expressed in terms of transfer functions. The wave number is corrected for convection (Doppler) effects and for visco-thermal dissipation by using Kirchhoff's damping coefficient α_0 [22, 23]:

$$k^{\pm} = \frac{k_0 + (1 - \mathrm{i})\alpha_0}{1 \pm M}, \qquad \alpha_0 = \frac{\sqrt{2\omega\nu}}{2ac_0}\left(1 + \frac{\gamma - 1}{\sqrt{\mathrm{Pr}}}\right). \tag{35, 36}$$

Here ν is the kinematic viscosity of air, a the radius of the pipe, and Pr is the Prandtl number of air. Peters [20] presented theoretical and experimental results for the correction of α_0 due to the interaction of the acoustic waves with the turbulent main flow. This correction is used to account for the effects of visco-thermal dissipation on the wave propagation.

The diaphragms being studied are slit-shaped diaphragms in a cylindrical pipe. Although this is a three-dimensional configuration the response of the configuration is expected to be governed by the two-dimensionality of the slit-shaped diaphragm. This makes a comparison to two-dimensional numerical simulations reasonable. Three diaphragms with varying apertures have been used. The aperture can be as large as 45, 27 or 11% of the pipe cross-sectional area. In Figure 12, one of the diaphragms is shown. The edge of the diaphragms is kept sharp (radius of curvature less than 10^{-5} m) and at the downstream side the aperture diverges with a bevel angle of 45°. This ensures a predictable vena contracta effect.

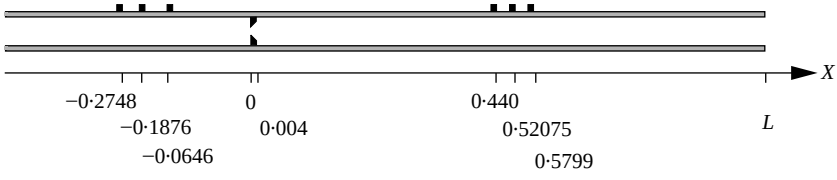

Figure 14. Microphone configuration used for the measurement at 793 Hz. Positions of the microphones ■ given in meters.

Downstream of the diaphragm the pipe has a length L. The air exits the set-up at the end of the pipe into the surroundings of the laboratory. At both sides of the diaphragm three or four pressure transducers are located. The position of the diaphragm is chosen as the reference point for the co-ordinate system. In Figure 13, the microphone positions that are used for the low-frequency experiments (77 Hz) are shown. In order to show the deviations from the quasi-steady model for higher frequencies, experiments have also been performed at a higher frequency (793 Hz). In Figure 14, the microphone positions for these experiments are shown. Additional data for the scattering matrix at low frequencies by means of two-load method are presented in a paper by Durrieu *et al.* [9] which is focused on the quasi-steady response of circular diaphragms and perforated plates. In all cases the position $x = 0$ corresponds to the upstream face of the diaphragm. This is the position at which the reflection and transmission coefficients are determined.

5.2. EXPERIMENTAL RESULTS FOR LOW FREQUENCIES

The results of the theoretical model are compared to experimental measurements of the reflection and transmission of acoustic waves by a diaphragm in a pipe. The experiments consisted in measuring the following complex quantities as functions of the Mach number:

$$R_1 = p_1^-/p_1^+, \quad T_{21} = p_2^+/p_1^+, \quad R_2 = p_2^-/p_2^+. \tag{37}$$

These measurements do no determine the response of the diaphragm separately but they determine the combined response of the diaphragm and pipe termination (open pipe end). However, all the information about the open pipe end is contained in the reflection coefficient R_2 and a lot of theoretical and experimental work has already been done on open pipe ends. Peters [20] presented an elaborate discussion on the open pipe end. The experimental data of Peters were used in the form of a fit. These data have been obtained in the ranges $0{\cdot}01 < M < 0{\cdot}2$ and $0{\cdot}01 < \mathrm{Sr} < 1$ which are close to the ranges of the present experiments. The magnitude of the reflection coefficient of the open pipe end is then described as proposed by Cargill [24]

$$|R| = (1 + \mathscr{A}M)(1 - (ka)^2/2), \tag{38}$$

where $\mathscr{A}$ is approximated by

$$\mathscr{A}(x) = \begin{cases} x^2/3, & 0 \leqslant x < 1, \\ \dfrac{2x-1}{3}, & 1 \leqslant x < 1{\cdot}85, \\ 0{\cdot}9, & 1{\cdot}85 \leqslant x, \end{cases} \tag{39}$$

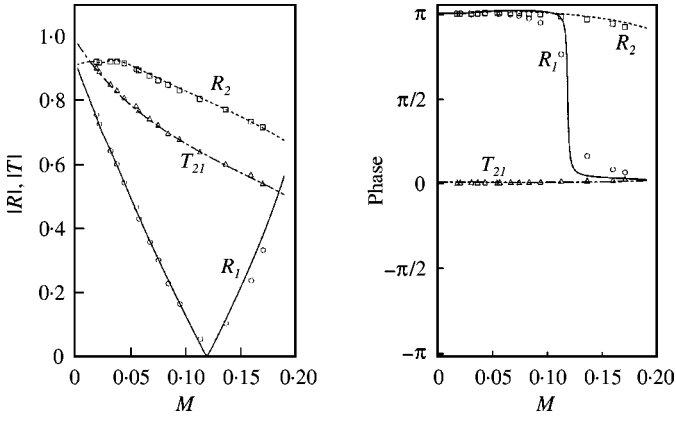

Figure 15. Comparison of experimentally measured reflection and transmission coefficients and theoretical predictions based on the compressible-flow model including the vena contracta effect. Diaphragm I, $f = 77$ Hz, $L = 2{\cdot}1959$ m.

in which

$$x = ka/M = (2\pi fa)/u_0 = 2\pi\,\mathrm{Sr}. \tag{40}$$

The phase of the reflection coefficient is presented in terms of an end correction δ_p which is approximated by

$$\frac{\delta_p}{a} = \begin{cases} 0{\cdot}2 + 0{\cdot}4x^2, & 0 \leqslant x < 1, \\ 0{\cdot}6, & 1 \leqslant x. \end{cases} \tag{41}$$

The contraction ratio used in the compressible-flow model of section 2.3 is estimated by

$$\Upsilon = \frac{\Upsilon_0}{\pi/(\pi+2)}\left(\frac{\pi}{\pi+2} + 0{\cdot}13M_j^2\right), \tag{42}$$

where Υ_0 is taken from Figure 8 at the average value of $h_d/h_p = S_d/S_p$ across the width of the diaphragm. The term between brackets is the correction for the compressibility of the flow and it is an accurate fit to the result of Chaplygin (shown in Figure 9).

In Figure 15, the prediction obtained from the compressible-flow model is compared to experimentally obtained values of R_1, T_{21}, and R_2 at a frequency of 77 Hz for the diaphragm with the largest aperture (diaphragm I, $S_d/S_p = 0{\cdot}45$). On the left, the magnitude of the coefficients is shown and on the right the phases of the coefficients are shown. The experimental results are the markers and the lines are the theoretical predictions from the compressible flow model. As can be expected, the results for R_2 (which are experimental data for the open pipe end) coincide with the fit to the results of Peters [20]. Also, the values of R_1 and T_{21} are in excellent agreement with our quasi-steady model. A similar agreement is evident in Figure 16. The frequency is again 77 Hz and the diaphragm used in this case has the smallest aperture (diaphragm III, $S_d/S_p = 0{\cdot}11$). In both cases, the quasi-steady approximation gives very accurate predictions for the acoustic response of the diaphragm. In the companion paper it is shown that the important parameter for the unsteadiness caused by the flow through the diaphragm is the Strouhal number based on the aperture height and velocity: $\mathrm{Sr} = fh_d/u_d$ with $u_d = (S_p/S_d)u_1$. In both experimental series, the highest value of the Strouhal number encountered is less than 0·05 which explains the validity of the

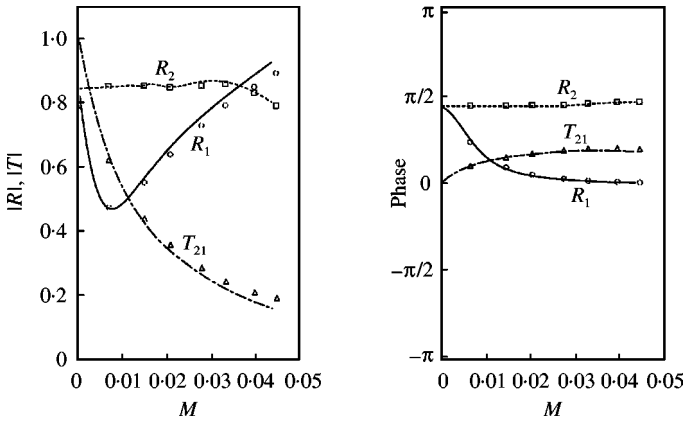

Figure 16. Comparison of experimentally measured reflection and transmission coefficients and theoretical predictions based on the compressible-flow model including the vena contracta effect. Diaphragm III, $f = 77$ Hz, $L = 5{\cdot}0069$ m.

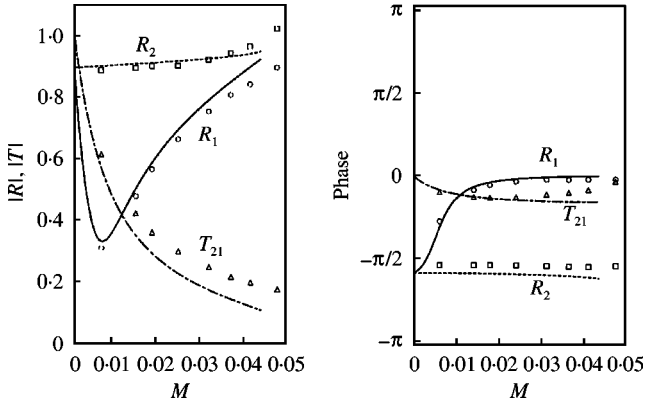

Figure 17. Comparison of experimentally measured reflection and transmission coefficients and theoretical predictions based on the compressible-flow model including the vena contracta effect. Diaphragm III, $f = 793$ Hz, $L = 0{\cdot}8089$ m.

assumption of quasi-steadiness. The excellent agreement between theory and experimental results at 77 Hz for both diaphragms I and III indicates that the three-dimensional effects due to the use of a circular pipe are negligible. The quality of this agreement is almost surprising in view of the crudeness of some assumptions in the model such as that of a very short turbulent mixing region downstream of the jet. This assumption was made implicitly by neglecting wall friction effects in equation (20) and heat transfer in equation (22). In reality, a long mixing region of at least 10 pipe diameters is expected before the fully developed turbulent pipe flow is established. However, the aeroacoustic behavior seems to be determined by the details of the jet flow rather than by the structure of the mixing region. When the frequency is raised to 793 Hz the results for diaphragm III are still in reasonable agreement with experimental results (see Figure 17). The difference between the results of theory and experiment is somewhat larger than in the low-frequency case, but this might only be due to inaccuracies in the fit for R_2. These inaccuracies affect the values of R_1 and T_{21} as well. When diaphragm III is replaced by diaphragm I the inaccuracies in R_2 are no longer the only source of inaccuracies. In Figure 18, the difference between results of theory and experiments can be seen to be significant as opposed to differences in the other three

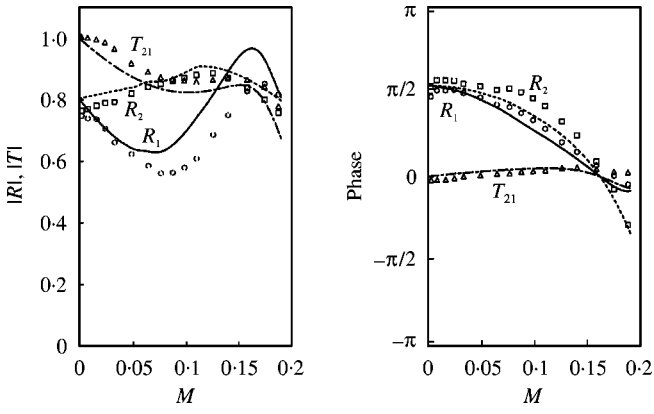

Figure 18. Comparison of experimentally measured reflection and transmission coefficients and theoretical predictions based on the compressible-flow model including the vena contracta effect. Diaphragm I, $f = 793$ Hz, $L = 1{\cdot}7651$ m.

cases. In fact, at the Mach number of 0·01 the Strouhal number is close to unity which implies that the flow through the diaphragm is essentially unsteady.

6. CONCLUDING REMARKS

In this paper, a study has been presented of the flow through a slit-shaped diaphragm in a pipe. This study consisted of analytical modelling and measurements. It has been shown that for acoustic perturbations the diaphragm can be acoustically characterized by the so-called scattering matrix. This matrix relates the outgoing waves to the incoming waves. In the case of an incompressible flow the matrix is shown to be symmetric. The symmetry of the matrix is destroyed by compressibility effects.

The models presented in this paper represent different approximations to the flow through the diaphragm. The focus has been on high Reynolds number and low Helmholtz number flows. In this case, the flow can be separated into two regions: a region of wave propagation (far upstream and far downstream of the diaphragm) and a source region (around the diaphragm). The source region can be considered compact and the effect of wave propagation can be neglected inside the source region. The production or dissipation of acoustic energy takes place in the source region. For $M_j \ll 1$ and $\mathrm{Sr} \ll 1$ the incompressible quasi-steady flow model of section 2.2 can be applied. When $M_j = \mathcal{O}(1)$ and still $\mathrm{Sr} \ll 1$ compressibility is important in the source region. For subsonic flows $M_j \leqslant 1$ the compressible quasi-steady flow model of section 2.3 can be used. When, on the other hand, $M_j \ll 1$ but now $\mathrm{Sr} = \mathcal{O}(1)$ the flow in the source region is essentially unsteady but can still be considered incompressible.

Both an incompressible and a compressible quasi-steady model of the flow through a diaphragm in a pipe have been presented. An important parameter in these models is the vena contracta factor Υ. The influence of the diaphragm geometry (S_d/S_p) as well as the influence of compressibility on the vena contracta factor have been discussed. An interpolation method is proposed to obtain Υ (as a function of both S_d/S_p and M_j) from limit cases $S_d/S_p \to 0$ and $M_j \to 0$ respectively. The predictions of the compressible-flow model are compared to low-frequency experimental results for reflection and transmission coefficients. The agreement between the model and the experiments is very good at a frequency of 77 Hz. This indicates that the crude assumptions used in the description of

the downstream turbulent mixing region are not crucial for the aeroacoustic response of the system. This response seems to be determined locally at the free jet formed by flow separation in the diaphragm. At a higher frequency of 793 Hz the experimental results diverge from the model predictions. The unsteadiness caused by the flow is expected to be important in that case because $\mathrm{Sr} = \mathcal{O}(1)$. The response of the diaphragm at low Mach numbers for $\mathrm{Sr} = \mathcal{O}(1)$ is discussed in a companion paper [11].

The focus has been on a rectangular aperture in order to enable a comparison with the results of two-dimensional numerical flow simulations as presented in the companion paper. Durrieu *et al.* [9] presented measurements for round orifices.

ACKNOWLEDGMENTS

Part of this research was sponsored by the Dutch Technology Foundation (project ETN33.2952) and Heinrich Gillet GmbH & Co. KG, Tenneco Automotive, Germany.

The authors wish to thank R. Prachen and J. Bruggeman for initiating the study of the effect of compressibility.

REFERENCES

1. J. Rayleigh 1896 *The Theory of Sound*. New York: Dover Publications Inc.
2. U. Ingard 1953 *Journal of the Acoustical Society of America* **25**, 1037–1061. On the theory and design of acoustic resonators.
3. U. Ingard and H. Ising 1967 *Journal of the Acoustical Society of America* **42**, 6–17. Acoustic non-linearities of an orifice.
4. D. Ronneberger 1967 *Acustica* **19**, 222–235. Experimentelle Untersuchungen zum akustischen Reflexionsfator von unstetigen Querschnittsänderungen in einem luftdurchströmrten Rohr.
5. D. W. Bechert 1980 *Journal of Sound and Vibration* **70**, 389–405. Sound absorption caused by vorticity shedding, demonstrated with a jet flow.
6. M. S. Howe 1984 *IMA Journal of Applied Mathematics* **32**, 187–209. On the absorption of sound by turbulence and other hydrodynamic flows.
7. A. Cummings and W. Eversman 1983 *Journal of Sound and Vibration* **91**, 503–518. High amplitude acoustic transmission through duct terminations: theory.
8. R. R. Parchen and J. C. Bruggeman 1995 *private communication.*
9. P. Durrieu, G. Hofmans, G. Ajello, R. Boot, Y. Auregan, A. Hirschberg and M. C. A. M. Peters 1999 *Journal of the Acoustical Society of America* (submitted). Quasi-Steady aeroacoustic response of orifices.
10. S. Rienstra 1983 *Journal of Sound and Vibration* **6**, 539–556. A small Strouhal number analysis for acoustic wave-jet flow-pipe interaction.
11. G. C. J. Hofmans, M. Ranucci, G. Ajello, Y. Auregan and A. Hirschberg 2000 *Journal of Sound and Vibration* **244**, 57–77. Aeroacoustic response of a slit-shaped diaphragm in a pipe at low Helmholtz number—2. Unsteady results.
12. M. Abom 1991 *Mechanical Systems and Signal Processing* **5**, 89–104. Measurement of the scattering-matrix of acoustical two-ports.
13. P. E. Doak 1998 *Acoustical Physics* **44**, 677–685. Fluctuating total enthalpy as a generalized acoustic field.
14. M. S. Howe 1998 *Acoustics of Fluid–structure Interactions*, Cambridge: Cambridge University Press.
15. L. S. G. Kovasznay 1953 *Journal of Aeronautical Science* **20**, 657–674. Turbulence in supersonic flow.
16. L. Prandtl and O. G. Tietjens 1934 *Fundamentals of Hydro- and Aeromechanics* New York: Dover Publications Inc.
17. R. D. Blevins 1984 *Applied Fluid Dynamics Handbook*. New York: Van Nostrand Reinhold Company Inc.

18. R. W. SEARS 1954 *General Theory of High Speed Aerodynamics*, Vol. VI. Princeton: Princeton University Press.
19. A BUSEMANN 1937 *Zeitschrift für Angewandte Mathematik und Mechanik* **17**, 73–79. Hodographenmethode der Gasdynamik.
20. M. C. A. M. PETERS, A. HIRSCHBERG, A. J. REIJNEN and A. P. J. WIJNANDS 1993 *Journal of Fluid Mechanics* **256**, 499–534. Damping and reflection coefficient measurements for an open pipe at low Mach number and low Helmholtz number.
21. M. ABOM and H. BODÈN 1988 *Journal of the Acoustical Society of America* **83**, 2429–2438. Error analysis of two microphone measurements in ducts with flow.
22. H. TIJDEMAN 1975 *Journal of Sound and Vibration* **39**, 1–33. On the propagation of sound waves in cylindrical tubes.
23. A. D. PIERCE 1989 Acoustics: An Introduction to its Physical Principles and Applications. New York: Acoustical Society of America.
24. A. M. CARGILL 1982 *Journal of Sound and Vibration* **83**, 339–354. Low frequency radiation from a jet pipe—a second order theory.